A New Approach to Durability Prediction for Fuel Tank Skins

M.A. Ferman,* W.H. Unger,† and C.R. Saff‡
McDonnell Aircraft Company, St. Louis, Missouri
and
M.D. Richardson§
Air Force Wright Aeronautical Laboratory, Wright-Patterson Air Force Base, Ohio

Fuel tank leakage has been a dangerous and costly problem, plaguing the aircraft industry and government with extensive maintenance efforts and lengthy aircraft tie-ups. A potential source of these leaks is believed to be premature fatigue cracks initiated from a newly recognized dynamic loading in addition to nominal spectrum fatigue loading. This new loading source results from fluid structure interaction dynamics between tank skins and fuel mass. Significant strain intensifications are produced, and because they occur at higher frequencies, they cause a reduced fatigue life. It is believed that this approach may help to explain why many instances of premature tank skin fatigue and leakage were not previously predicted by maneuver spectrum fatigue methods. This should provide an improved design approach to minimize fuel leakage from fatigue cracks.

Nomenclature

a	= tank length
b	= tank height
BCM	= Boundary Condition Method
dA	= incremental area
dV	= incremental volume
D	= deflection, and damping
f	= frequency, Hz
M	= mass
K	= stiffness
Q	= force
T,t	= transfer function, time
u,v,w	= velocity in x, y, z directions, respectively
x	= distance along tank
y	= vertical height and direction
z	= lateral direction
β	= decay rate
δ	= deflection
ϵ	= strain
η	= modal deflection coordinate
ρ	= density
ϕ,Φ	= mode shapes
ω	= frequency, rad/s
[ ]	= square, rectangular matrices
⌊⌋	= row matrix
{ }	= column matrix

Introduction

THIS effort is the result of an Air Force contract[1] aimed at extending earlier McDonnell Aircraft Company (MCAIR) work[2] into a practical approach for durability prediction of flat, bottom tank panels. MCAIR's interest was triggered by two incidences in 1974-1975; namely, 1) a tank skin was cracked during a slosh and vibration test, and 2) a wing skin was cracked in nominal high-speed flight. Both incidences were traced to mechanisms present only when fluidic effects were considered. The slosh test crack was initiated from an overstress condition resulting from the slosh frequency matching a resonance of a panel that was lowered due to fuel mass effect. In the dry case, the panel frequency was much higher, thus no significant strain would have been encountered at the slosh frequency. The wing crack was believed to result from a type of panel flutter produced by coupling of wing skin vibration and wing fuel mass oscillation.

MCAIR initiated an Independent Research and Development Program (IRAD) in 1975 to evaluate the mechanisms behind these phenomena, culminating initially in several applications in Ref. 2. The potentially damaging loads induced by coupled fluid-structure oscillations were recognized as a major area to concentrate the present effort. Fluid coupling reduces the nominally higher panel frequency that places the panel in regions of more intense excitation. Reductions of up to 5 to 1 were found. Likewise, it was found that panels along tank bottoms and lower side areas could be excited more intensively at higher fluid levels in environmental vibration because the fluid head also acts as a driving force. Cases of strain growth of up to 12 times the dry case were found as well. These effects combine to reduce fatigue life, particularly when combining these newly observed loads with those normally encountered in spectrum fatigue design. The authors believe that this new loading source may explain why the use of maneuver load spectrum did not predict in-service failures in Ref. 3. MCAIR has continued IRAD efforts since that time to extend this work.

Mutual Air Force interest in fuel tank fatigue and leakage culminated in Contract F33615-81-C-3217, "Fuel Tank Durability with Fluid-Structure Interction Dynamics," with MCAIR from 1980 to 1982.[1] This expanded the formative work of Ref. 2 into a more general technique combining panel-fluid vibration and response with a fatigue life prediction method into a single-pass, automated procedure. Experiments were performed to verify all aspects. Results of the contracted effort are summarized herein.

Analytical Effort

The analytical effort consisted of mechanizing and expanding the initial pieces of the process into an overall technique and computer code. Figure 1 shows a flowchart of the code. This technique required development of a reliable and ac-

Presented as Paper 85-0602 at the AIAA/ASME/ASCE/AHS 26th Structures, Structural Dynamics and Materials Conference, Orlando, FL, April 15-17, 1985; received June 17, 1985; revision received Dec. 11, 1985.

*Senior Staff Engineer.
†Senior Engineer.
‡Technology Specialist.
§Project Engineer.

curate vibration program with fluid-structure interaction, see the first block in Fig. 1. Computation of the response of the panel-fluid system to environmental vibration is shown in block 2. This was developed and coupled to the vibration step. Block 3 shows the fatigue prediction code that was developed. There data are taken from the first two parts and lifetime estimates for a given situation to establish.

Vibration

The vibration technique is an enhanced version of that developed in Ref. 2 using a Rayleigh-Ritz method to couple the fluid and structural oscillations. This is summarized in the form

$$[M^P_{JJ} + M^F_{JK}]\{\ddot{\delta}_K\} + [\omega^2_{JJ} M^P_{JJ}]\{\delta_K\} = 0 \tag{1}$$

where M^P is the panel mass, M^F the fluid mass, ω the dry panel vibration frequency, and δ the panel amplitude. For reasons of simplicity, we concentrated on solving simple, flat, pinned-pinned and fixed-fixed panels, with the latter being the more useful for tests and a more practical starting point. Note that only fluid mass effects appear in Eq. (1). This results from the assumption of an incompressible fluid, and also because low-frequency slosh-type oscillations are not considered herein. The panel mass terms are typical; i.e.,

$$M^P_{JJ} = \iint \rho_p t_p (\phi^P_j)^2 \mathrm{d}A \tag{2}$$

where ρ_p is the panel mass, t_p the panel thickness, ϕ^P the dry panel mode shape, $\mathrm{d}A$ the incremental area, and j the mode number. The fluidic mass terms appear as

$$M^F_{JK} = \rho_F \iiint (\phi^u_J \phi^u_K + \phi^v_J \phi^v_K + \phi^w_J \phi^w_K)\mathrm{d}V \tag{3}$$

where ρ_F is the fluid density, $\mathrm{d}V$ the incremental volume, and ϕ^u, ϕ^v, and ϕ^w the velocity profile terms in each of the principal directions throughout the tank. Note that the velocity profiles are cross-coupled via subscripts J and K, whereas panel mass is diagonal. This mass-coupling influence combines the normally uncoupled panel modes. The velocity profiles were developed from the idea that each profile must match panel velocities properly and yet satisfy fluid dynamic requirements. An example of this would be to show that the profile u perpendicular to a pinned ended side panel, Fig. 2, would have the form

$$u = \dot{\delta}_{mn} \phi^u_{mn} \tag{4a}$$

$$\phi^u_{mn} = \sin\frac{m\pi y}{b} \sin\frac{n\pi z}{c} \left(\frac{e^{-\beta x} - e^{\beta(x-2a)}}{1 - e^{-2\beta a}} \right) \tag{4b}$$

$$\beta = \pi \sqrt{\frac{m^2}{b^2} + \frac{n^2}{c^2}} \tag{4c}$$

where m,n are wave numbers, x the distance along the tank, y and z the distances along the vertical and lateral directions, b and c the panel size, and a the tank length. Observe that the fluid velocity profile matches the panel at the left and then decays along the tank to a zero value at the far end to satisfy the rigid wall conditions there. In Ref. 2, there were two fluidic methods used to define the velocity profiles. However, in the expanded version of Ref. 1, use was made mainly of one technique only, namely, the Boundary Condition Method (BCM).

Response

The response portion was aimed at defining panel-fluid response for various levels of sine and random excitation considering moving base motion. The response equation, in terms

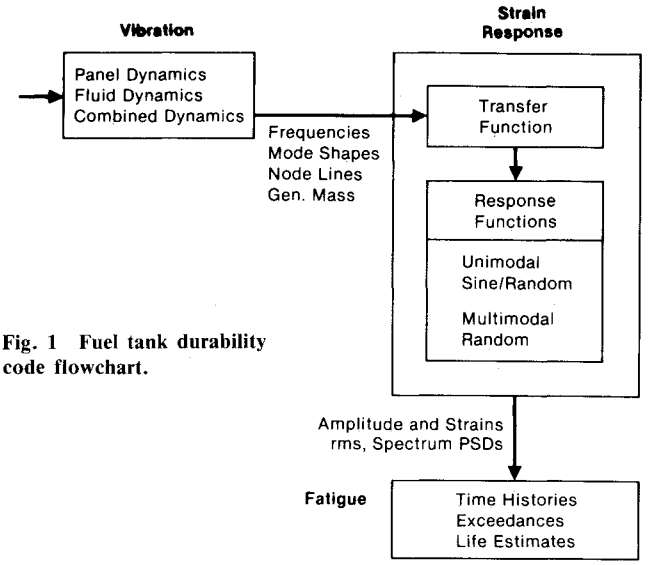

Fig. 1 Fuel tank durability code flowchart.

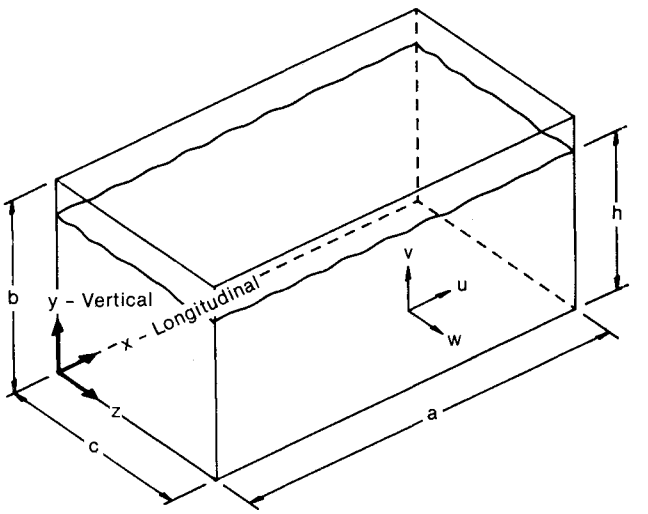

Fig. 2 Tank geometry and parameters.

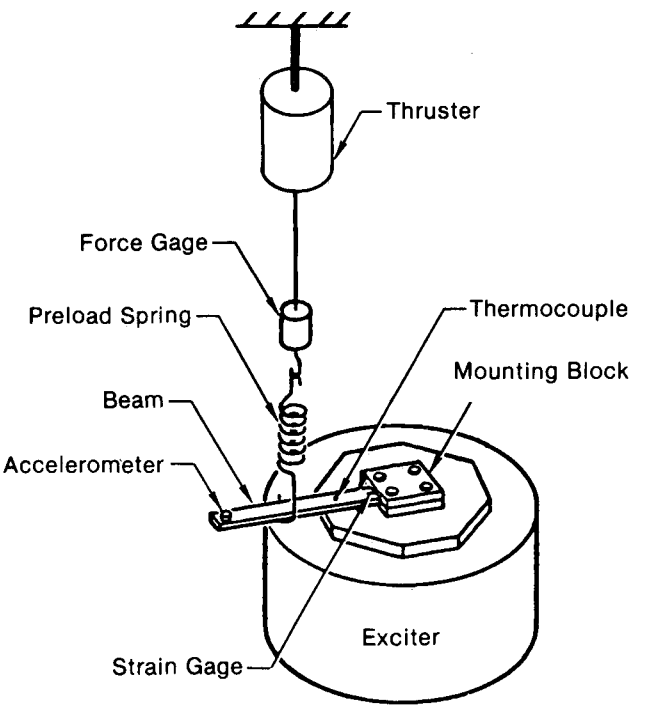

Fig. 3 Setup for beam bending tests with oscillatory preload.

of normal modes, is given in matrix format as follows:

$$[\tilde{M}^T]\{\ddot{\eta}_p\} + [D^T]\{\dot{\eta}_p\} + [\tilde{K}^T]\{\eta_p\} = \{\tilde{Q}\} \tag{5}$$

where

$$[\tilde{M}^T] = [\Phi_p]^T [M_{JK}^T] [\Phi_p] \tag{6a}$$

$$[\tilde{K}_{JJ}^T] = [\omega_{cJ}^2] [\tilde{M}_{JJ}^T] \tag{6b}$$

$$[\tilde{D}_{JJ}^T] = [2\tilde{M}_{JJ}^T \omega_{cJ} \zeta_{cJ}] \tag{6c}$$

$$\{\tilde{Q}\} = [\Phi_p]^T \{M_{JB}^T\} \ddot{\delta}_B \tag{6d}$$

where ω_c is the coupled fluid-structure oscillation frequency from Eq. (1) and Φ_p the coupled mode shape. The normal mode coordinates are related to panel deflection D by the relation

$$\{\delta\} = [\Phi_p]\{\eta_p\} \tag{7a}$$

$$\{D\} = [\Phi^P]\{\delta\} = [\Phi^P][\Phi_P]\{\eta_P\} \tag{7b}$$

One of the unique portions of the equations are the forces on the right-hand side of Eq. (5). Since we are interested in environmental vibration, the analogy is one of moving base excitation. Thus, based on this concept, the forces $\{\tilde{Q}\}$ of Eq. (6d) reflect a dynamic mass M_{JB}^T with both fluidic and structural components, i.e.,

$$M_{JB}^T = M_{JB}^P + M_{JB}^F \tag{8}$$

where these mass terms are similar to those comparable mass terms in the basic vibration equation, Eq. (1); namely, they have the form

$$M_{JB}^P = \iint \rho_P t_P \Phi_J^P \, dA \tag{9a}$$

$$M_{JB}^F = \iiint \rho_F (\Phi_J^u \phi_B^u + \phi_J^v \phi_B^v + \phi_J^w \phi_B^w) \, dV \tag{9b}$$

where ϕ_B^u, ϕ_B^v, and ϕ_B^w are additional velocity profiles satisfying the moving base condition, see Ref. 1. It is convenient to express all panel amplitude and strain response in terms of transfer function and force. Thus, using Eq. (5) as a base, we can find the normal mode coordinate transfer function $T_{n_{JJ}}$ as

$$T_{n_{JJ}} = \frac{1}{-\omega^2 \tilde{M}_{JJ}^T + 2i\tilde{M}_{JJ}^T \tilde{\zeta}_J \omega_{c_J} \omega + \omega_{c_J}^2 \tilde{M}_{JJ}^T} \tag{10}$$

We can define the amplitude T_D and strain transfer function T_ϵ as follows:

$$[T_D] = [\phi^P][\Phi_P][T_n] \tag{11a}$$

$$[T_{\epsilon_y}] = \left[-\left(\frac{t}{2}\right)\frac{\partial^2 \phi^P}{\partial_y^2}\right][\Phi_P][T_n] \tag{11b}$$

where the subscript ϵ_y refers to strain in the y direction on the end panel of Fig. 2. Thus, if the base coordinate motion is defined, the amplitude and strain response can be defined via

$$\{D\} = [T_D]\{\tilde{Q}\} \tag{12a}$$

$$\{\epsilon_y\} = [T_{\epsilon_y}]\{\tilde{Q}\} \tag{12b}$$

For example, if we are interested in sine response at resonance, the strain in a unimodal case is

$$\epsilon_{yJ} = -\frac{t}{2}\frac{\partial^2 \phi^P J}{\partial_y^2}\frac{\phi P\{M_{JB}^T\} g U_B}{2\tilde{M}_T \zeta_c \omega_{cJ}^2} \tag{13}$$

where U_B is the base acceleration in gs. The technique can handle sine and random input for unimodal and multimodal cases. Both broadband and narrowband random-type data can be used. As noted above, a closed-form version can be used for unimodal sine, as well as for unimodal random sine with white noise input.

Fatigue

In the third part of the code, fatigue life is calculated based on an accumulative damage concept, such as the Palmgren-Miner method in Refs. 4 and 5, and employs a cycle-by-cycle computation of damage per Ref. 6. Two methods are included: Cyrus and Beiger. Beiger is the more thorough spectrum technique of Ref. 7, extended to the higher frequencies used in this application. A random time history from the psd data is used to obtain cycle-by-cycle damage. Cyrus, on the other hand, is slightly less rigorous and uses the rms value of the strain psd to estimate damage from the strain-to-failure curve of the material. Both routines employ a modification of nominal pure axial fatigue to account for pure bending, pure axial, and cases mixing both.

Experimental Setup

Lab tests were conducted for a series of beams to validate strain-to-failure data curves for use in panel fatigue tests. The panel tests were made in a series where many parameters were varied to provide a wide matrix of results to validate the theory presented herein.

The setup for the beam bending coupon tests is shown in Fig. 3. The beams were 7075 T-6 aluminum alloy strips, 1.5 in. wide by 0.125 in. thick, and 24 in. long. The exposed beam length was varied from 6 to 20 in. in the tests. The beams were cantilevered to a block attached to a shaker head so that moving base excitation could be employed. Preload was applied using a soft spring attached near the cantilever root to minimize deflection. In some cases, static preload and low-frequency sinusoidal excitation were combined by attaching a long stroke exciter (thruster) between the preload spring and the ground. This setup provided for three types of loading, and their related fatigue were obtained: 1) pure dynamic bending fatigue, 2) a combination of bending fatigue with static preload, and 3) combinations of bending with static preload and low-frequency sinusoid.

Beam strains were measured at the beam's center outer fiber near the root. An accelerometer was mounted on the free end of the beam and used to measure response. It was also correlated with the strain gage for backup in the event of strain-gage failure. The accelerometer provided a convenient weight to control the vibration frequency and root strain due to the dynamic mass effects.

All experimental points for a specific condition lie within a very narrow bandwidth and show very little scatter, thereby establishing the credibility of the strain fatigue data used in the panel fatigue tests. The values of the experimental points are shown with the test correlation in subsequent figures.

The panel test configuration is shown in Fig. 4. It consists of a tank constructed of ½-in. aluminum plates welded together with the top and bottom open. A bottom test panel of 10×16 in. was attached to a flange on the tank. A "picture frame" retainer was used to secure the panel to the tank to ensure a fixed-edge condition. A thick plexiglass top was used to close off the tank, but it allowed viewing of the fluid motions. The bottom test panels consisted of 7075 T-6 aluminum with thicknesses of 0.032, 0.040, and 0.063 in. Fluid depths of up to 11 in. were used. The tank was attached to a shaker head so that moving base excitation could be achieved, with input acceleration levels varying from 0.1 to 2.5g rms. Four strain gages were mounted near the panel edges at the midpoints of the sides and at a corner location, as shown in the figure. An accelerometer was used for frequency and mode shape identification. Cases with static

pressure were also run so that static preload could be induced.

Fixed-edge, wetted panel fatigue results were obtained from the panel tests. Prior to fatigue runs, vibration and response surveys were made to ensure knowledge of the panel dynamic properties. The test data encompass frequency variation with fluid depth, static pressure, and input excitation, along with strain variation with pressure and input excitation. Trends indicate that as fluid depth increases, the resonant panel frequency increases. Increased fluid frothing or emulsifying accompanies increased excitation levels. The test results also indicate a sharp reduction of durability when combining static pressure and dynamic excitation. The fatigue test results are shown with the test correlation results in later figures. Some of the experimental strain response results are shown in the figures in the next section.

Correlation of Theory and Experiment

The fatigue theory accurately predicts the beam coupon test results as shown in Figs. 5-7. Figure 5 shows the results

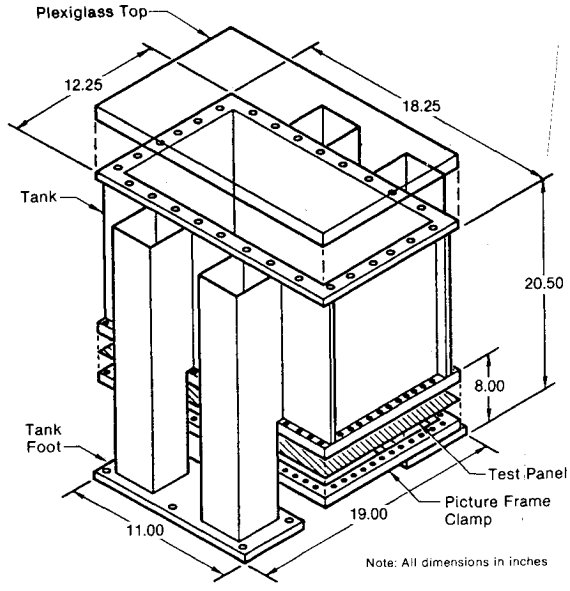

a)

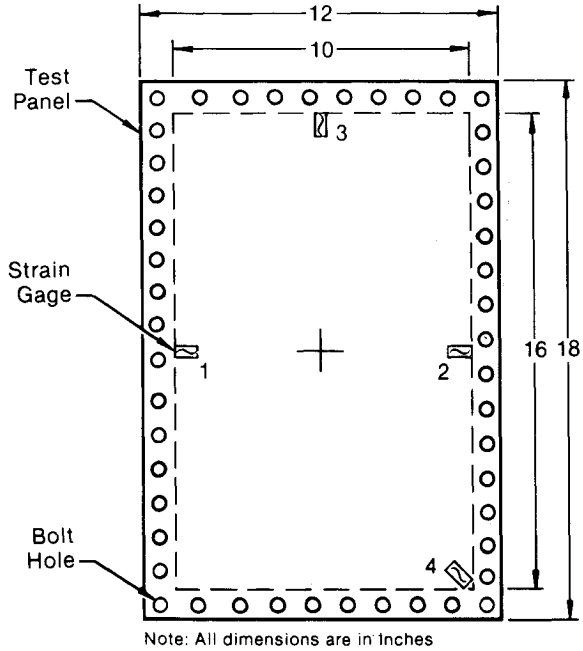

b)

Fig. 4 Panel test set-up: a) tanks, and b) panel.

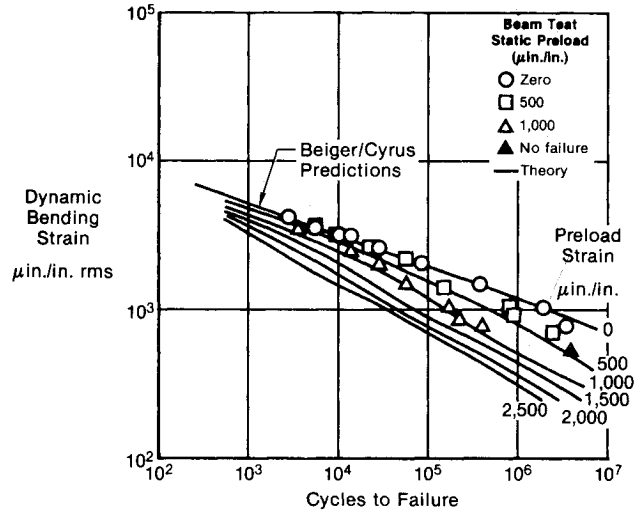

Fig. 5 Comparison of measured and predicted beam fatigue—sine excitation.

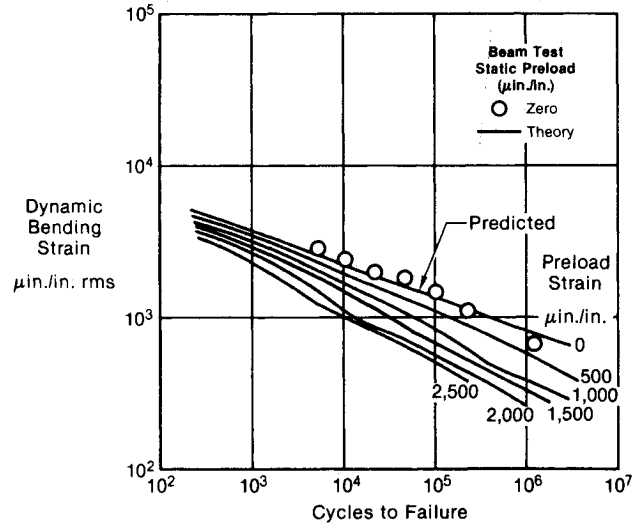

Fig. 6 Comparison of measured and predicted beam fatigue—random excitation.

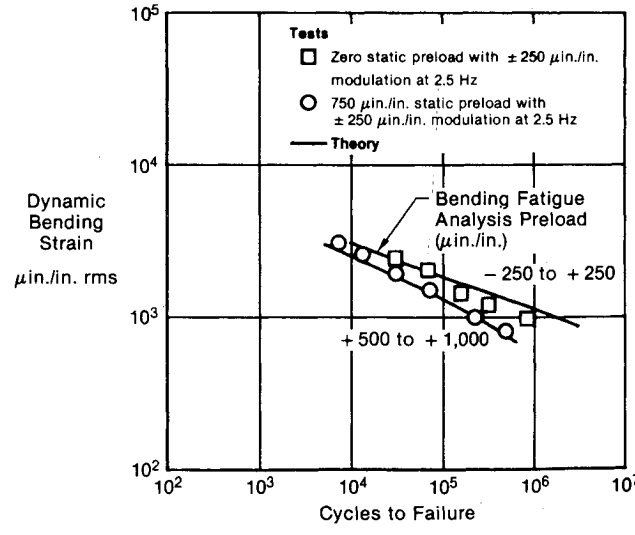

Fig. 7 Comparison of measured and predicted beam bending fatigue results with both high- and low-frequency sine input.

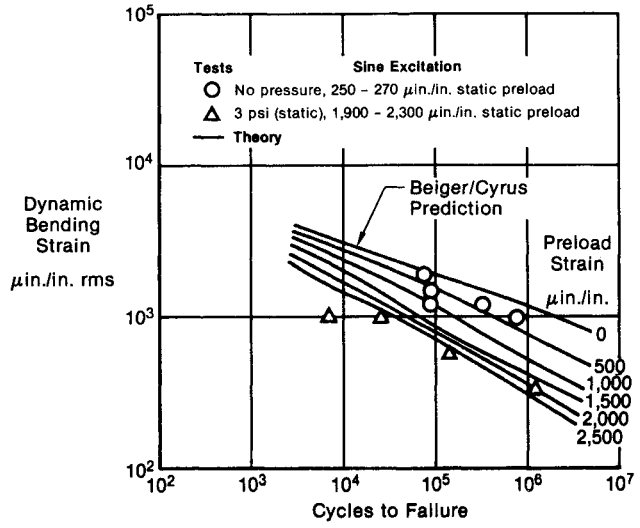

Fig. 8 Panel fatigue results: effect of internal pressure and panel thickness = 0.063 in.

Symbol	Panel Thickness (in.)	Static Preload Range (μin./in.)
	0.063	250 - 270
	0.040	300 - 770
	0.032	300 - 380
	0.032 Stiffened panel	430
	No failure dry	
	0.032 Random excitation	720

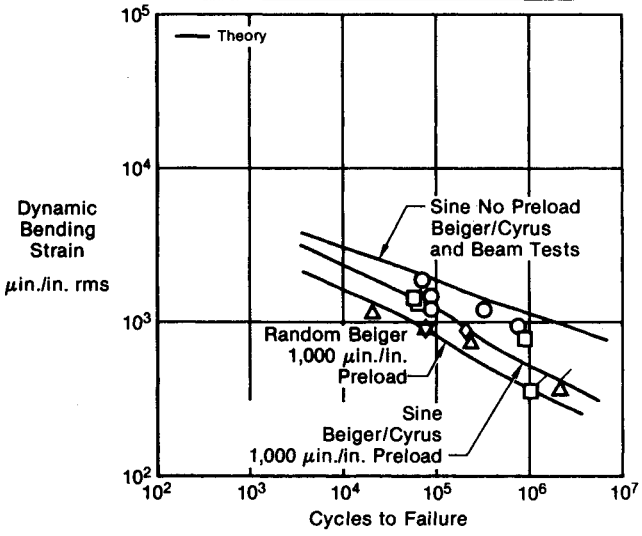

Fig. 9 Panel fatigue results, no internal pressure.

for a series of beam tests for dynamic excitations using sine input with various preload values. Static preloads for the tests were varied up to 1000 μin./in. rms, while theory is shown through 2500 μin./in. Good correlation is shown. The higher preload is required for the panel tests and will be more significant in those correlations.

Figure 6 shows a comparison of similar data for narrow-band random input. The only measured data in this figure is for zero preload and it compares well against predictions given herein for that preload value.

Figure 7 shows a comparison of measured and predicted beam bending fatigue results for combined high- and low-frequency sine inputs. In one case, the low-frequency sine input modulated the preload around ±250 μin./in., while in

Symbol	Panel Thickness (in.)	Fluid Depth (in.)
	0.032	11.0
	0.040	11.0
	0.063	11.0
	0.032	8.0
	0.040	8.0
	0.063	8.0
	0.032	4.0
	0.040	4.0
	0.063	4.0

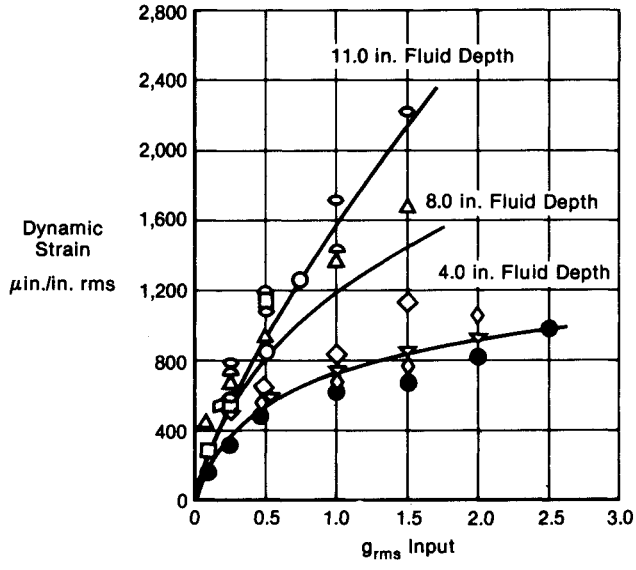

Fig. 10 Dynamic strain vs excitation level—sine excitation.

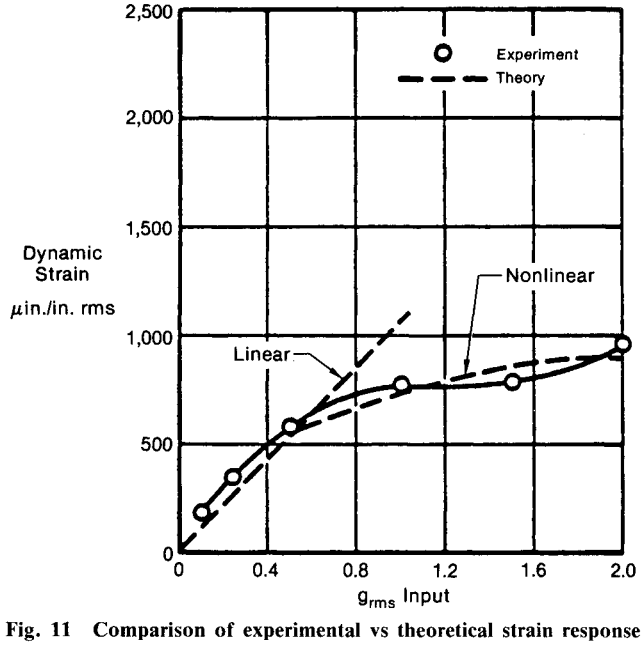

Fig. 11 Comparison of experimental vs theoretical strain response sine excitation; panel thickness = 0.063 in., fluid depth = 4.0 in.

the second case the same modulation was applied to a beam under a static preload of 750 μin./in. Good correlation is seen between the theory and experiment.

Panel fatigue predictions also correlated well with the panel test results for linear and nonlinear cases as shown in Figs. 8 and 9. The authors' test results vs predictions of the pressure effects on panel fatigue life are compared in Fig. 8. Here all results of the 0.063 panel test are plotted and clearly

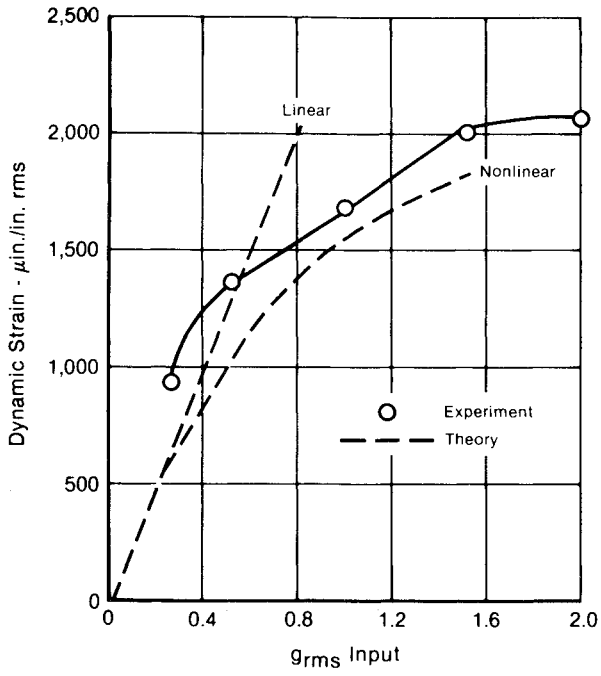

Fig. 12 Comparison of experimental vs theoretical strain response sine excitation; panel thickness = 0.063 in., fluid depth = 11.0 in.

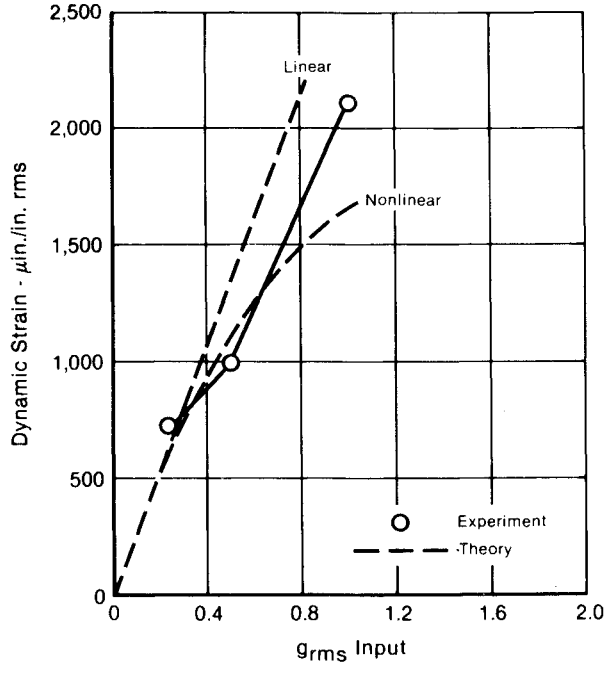

Fig. 13 Comparison of experimental vs theoretical strain response sine excitation; panel thickness = 0.063 in., fluid depth = 11.0 in.

indicate the sharp reduction of fatigue life due to static pressure. The fatigue life predictions were fairly accurate because the panel response was sinusoidal for both sets of tests.

The results of all unpressurized tests are plotted in Fig. 9. The theoretical fatigue results are shown for sine inputs with 0 and 1000 μin./in. preload, and for random input with 1000 μin./in. preload. The theoretical results bracket the test results for all 0.063 panels while showing too long of a life for the thinner panels. The random prediction shows a life that is too short. The panel tests fall within the two predictions, as they should, because a complex sine response was noted in the thinner panels and is somewhere between the unimodal sine and unimodal random case.

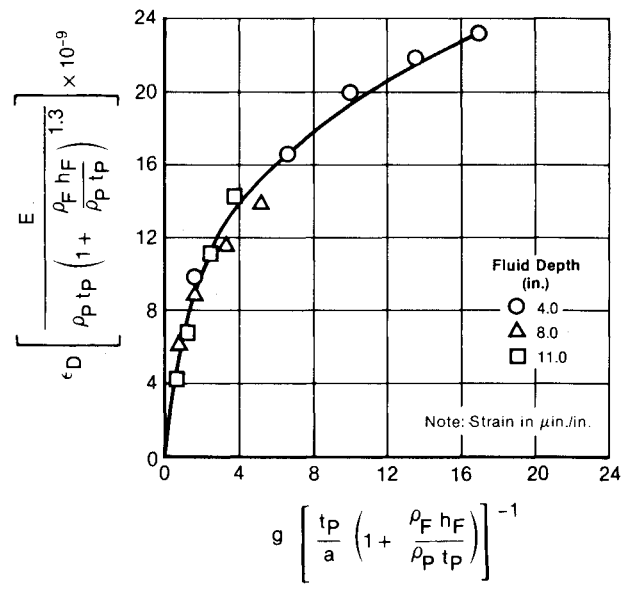

Fig. 14 Dynamic strain parameter vs input g parameter, mean strain at fluid depth.

One of the 0.032-in. panels was stiffened by adding two mechanically fastened "C" channel beams. This failed at a longer time than the test data would suggest for the comparable condition for an unstiffened 0.032-in. panel. Two "no failure" cases for dry panels were run to show that dry panels would not fail within the range of test conditions, as shown in Fig. 9. This emphasizes the loss of durability by fluid-structure interaction.

If panel fatigue can be predicted with reasonable accuracy from measured strain response, then the key to a successful approach is accurate prediction of panel strain response. Figure 10 shows results of the experimental strain response data for the panels presented herein. Note the significant strain growth vs base excitation and also from increased fluid depth. Linear predictions of panel strain and fatigue were reasonably reliable using an analytical closed-form approach. For the nonlinear region, a semi-empirical method (iterative) was used when the deflection exceeded one panel thickness. Linear and nonlinear strain responses are compared with predictions in Figs. 11-13 for some typical cases. It can be seen that the panels have a linear region where increases in excitation produce a corresponding increase in strain response. Also, all exhibit nonlinear regions where strain response does not follow the linear increase in excitation. There appears to be a linear region below input levels of 0.3-g rms for all cases. For the lower fluid depths, the transition from linear to nonlinear regions is quite apparent; however, it is not as apparent at the higher fluid depths.

Design Parameters

As noted earlier, the strain response is the key to establishing both strain level and fatigue life. In the resonant strain response data of Fig. 10, the essential factors for fatigue are given; namely, strain vs base excitation for three fluid depths and three thicknesses. When combined with exposure time at resonance, the life-cycle time is defined. Thus, the authors attempted to reduce these data into a generalized chart of broader applicability.

Nondimensional data forms were developed to aid in design selection without using analysis. Figure 14 shows one chart collapsing the data of Fig. 10 into a simple curve. The abscissa relates the dynamic excitation levels to fluid and panel properties, while the ordinate relates panel strain to similar properties. The terms used are: ϵ_d, dynamic strain; g, input gs of vibration; t_p, panel thickness; h_f, in fluid depth; ρ_f, fluid density; ρ_p, panel density; a, panel width; and E,

panel bending modulus. This applies to water, but is probably quite similar for fuel because of the nondimensional method used. The dynamic strain could be determined from this figure for a given panel and fluid for a given excitation level so that fatigue could be assessed for an exposure time.

Conclusion

It is the authors' belief that a new concept for fuel tank durability is in the process of being developed herein and represents a significant first step toward that goal. The recognition of the existence of the complex fluid-structure oscillation influence and its induced loading is a major departure from prior techniques, and the idea of combining both this loading and the nominal spectrum fatigue is a major new breakthrough. It is quite possible that some of the prior leakage problems stemmed from the cracks induced by these combined loads, however, this was neither identified nor included previously. While more work is needed to fully develop the method, it is hoped that others will now take a new look at the problem. In 1984, the Air Force initiated a second contract with McDonnell entitled "Analysis of Fuel Tank Dynamics for Complex Configurations." The research under the new contract will expand this original pioneering effort into more complex cases: single and parallel panels featuring flat, curved, and stiffened designs will be evaluated; and at least one tank of more general design having several flat and curved panels with a skin-stringer-frame-design will be considered.

Acknowledgments

Significant contributions to this effort were made by Mr. C.H. Perisho, Dr. N.H. Zimmerman, and Mr. C.N. Smith of McDonnell's Structural Dynamics Department; Mr. K. Sanger of McDonnell's Structural Research Department; and Messrs. M.H. Hieken, R.W. Merkle, H.J. Bieniecki, B. Scott, E. Bauer, and L. Rudolph of McDonnell's Dynamics Laboratory.

References

[1]Ferman, M.A., Unger, W.H., Smith, C. M., and Saff, C. R., "Fuel Tank Durability with Fluid-Structure Interactive Dynamics," AFWAL TR-82-3066, Sept. 1982.

[2]Ferman, M.A. and Unger, W.H., "Fluid-Structure Interaction Dynamics in Aircraft Fuel Tanks," *Journal of Aircraft*, Vol. 16, Dec. 1979.

[3]Krauter, R., "Results of F-4 Cavity Fatigue Tests," USAF-TM-ENS-76-03, July 1976.

[4]Palmgren, A., "Die Lebensdaur Von Kugellagern," *Z. Verein Deutsches Ingenieure*, Vol. 68, 1924, pp. 339-341.

[5]Miner, M.A., "Cumulation Damage in Fatigue," *Journal of Applied Mechanics*, Vol. 12, Sept. 1945, p. A-159.

[6]Impellizzeri, L.F., "Cumulation Damage Analysis in Structural Fatigue," *Effects of Environmental and Complex Load History in Fatigue Life*, ASTM, STP 462, American Society for Testing Materials, 1970, pp. 40-68.

[7]Dill, H.D. and Young, H.T., "Stress History Simulation," AFFDL TR-76-113, Vol. 1, March 1967.